High-spin structure and intruder excitations in ^{36}Cl

S. Aydin,[1,2,*] F. Recchia,[2] M. Ionescu-Bujor,[3] A. Gadea,[4,5] S. M. Lenzi,[2] S. Lunardi,[2] C. A. Ur,[2] D. Bazzacco,[2] P. G. Bizzeti,[6] A. M. Bizzeti-Sona,[6] M. Bouhelal,[7] G. de Angelis,[4] I. Deloncle,[8] E. Farnea,[2] A. Gottardo,[2,4] F. Haas,[9] T. Huyuk,[5] H. Laftchiev,[10] D. Mengoni,[2,11] R. Menegazzo,[2] C. Michelagnoli,[2] D. R. Napoli,[4] E. Sahin,[4] P. P. Singh,[4] D. Tonev,[10] and J. J. Valiente-Dobón[4]

[1]*Aksaray University, Department of Physics, 68100 Aksaray, Turkey*
[2]*Dipartimento di Fisica e Astronomia dell'Universitá and INFN, Padova, Italy*
[3]*National Institute for Physics and Nuclear Engineering, Bucharest, Romania*
[4]*INFN-Laboratori Nazionali di Legnaro, I-46020 Legnaro, Italy*
[5]*Instituto de Física Corpuscular, CSIC-Universidad de Valencia, Valencia, Spain*
[6]*Dipartimento di Fisica dell'Universitá and INFN Sezione di Firenze, Firenze, Italy*
[7]*Laboratoire de Physique Appliquée et Théorique, Université de Tebessa, Algeria*
[8]*IPNO, IN2P3/CNRS et Université Paris-Sud, Orsay, France*
[9]*IPHC, IN2P3/CNRS, Université de Strasbourg, Strasbourg, France*
[10]*Institute for Nuclear Research and Nuclear Energy, BAS, Sofia, Bulgaria*
[11]*University of the West of Scotland, Paisley, United Kingdom*

(Received 30 August 2011; revised manuscript received 25 June 2012; published 30 August 2012)

Excited states up to $J^\pi = 11^-$ at 10 296 keV and $J^\pi = 10^+$ at 10 707 keV have been populated in the odd-odd ^{36}Cl nucleus using the ^{24}Mg(^{14}N,2p) fusion-evaporation reaction at $E_{\rm lab} = 31$ MeV. Twenty new states and 62 new γ transitions have been identified by employing γ-γ and γ-γ-γ coincidences. Lifetimes have been investigated by the Doppler shift attenuation method. The experimental data have been compared with the results of large-scale shell-model calculations performed using different effective interactions and model spaces allowing particle-hole excitations across the $N = Z = 20$ shell gap.

DOI: 10.1103/PhysRevC.86.024320 PACS number(s): 21.10.Re, 23.20.Lv, 21.60.Cs, 21.10.Hw

I. INTRODUCTION

Nuclei in the *sd* shell are a fundamental testing ground for many basic models of nuclear structure. Several interesting phenomena can be studied as a function of the angular momentum in this mass region such as clusterization, shape coexistence, and proton-neutron interaction, as well as the interplay between collective and single-particle motion. The ^{36}Cl nucleus, with one neutron and three proton valence holes with respect to the doubly magic ^{40}Ca, has been studied extensively in the past with the aim of elucidating the role of intruder particle-hole *sd*-*fp* cross-shell configurations in the structure of *sd*-shell nuclei [1–10].

In previous works ^{36}Cl has been populated via stripping and/or pick-up reactions ^{35}Cl(d,p) [1–4], ^{37}Cl(p,d) [5,6], ^{37}Cl(^{3}He,α) [7,8], ^{2}H(^{35}Cl,p) [9,10], and ^{33}S(α,p) [11]. Only low and medium spin states up to $J = 7$ were observed [4,12–14] as a consequence of the use of light projectiles and of the limited sensitivity of the detection systems. The availability of large high-resolution γ-ray spectrometers has recently renewed the interest in studying medium- and high-spin states of light nuclei in the $A = 30$–40 mass region [15–17].

An experiment has been performed at the XTU-TANDEM accelerator of Laboratori Nazionali di Legnaro to investigate the high-spin structure of nuclei around mass 35. In this paper the results on the odd-odd nucleus ^{36}Cl are reported. The experimental details, the data reduction, and the analysis procedure are presented in Sec. II. In Sec. III the newly established level scheme is given and the lifetime measurements are reported. Section IV deals with the discussion of the experimental data in the framework of shell-model calculations. The results obtained in this work are summarized in Sec. V.

II. EXPERIMENTAL DETAILS AND DATA ANALYSIS

High-spin states of ^{36}Cl have been populated via the fusion-evaporation reaction ^{24}Mg(^{14}N,2p)^{36}Cl at 31 MeV bombarding energy. A ^{14}N beam, delivered by the LNL XTU-Tandem accelerator impinged on the target with an average beam current of 5 pnA. The 99.7% isotopically enriched ^{24}Mg target, 1 mg/cm^2 thick, was evaporated on a 8 mg/cm^2 gold layer. The γ rays emitted in the reaction were detected using the 4π-GASP array [18] composed of 40 Compton-suppressed large-volume, high-purity Ge detectors arranged in seven rings at different angles with respect to the beam axis. Events were collected when at least two germanium detectors fired in coincidence. Energy and efficiency calibrations were performed with standard γ-ray sources of ^{56}Co and ^{152}Eu.

The data were sorted into a symmetric γ-γ-γ cube, a symmetric γ-γ matrix, and seven asymmetric matrices having the detectors at 34°, 60°, 72°, 90°, 108°, 120°, 146°, respectively, on the first axis and all detectors on the second axis. The symmetric matrices have been used to study γ-γ coincidence relationships for the construction of the level scheme, while the asymmetric matrices were used to obtain information about the γ transition multipolarities and for lifetime determinations.

From previous studies several low-lying states in ^{36}Cl are known to have lifetimes longer than a few picoseconds [13,14].

*01sezgin@gmail.com

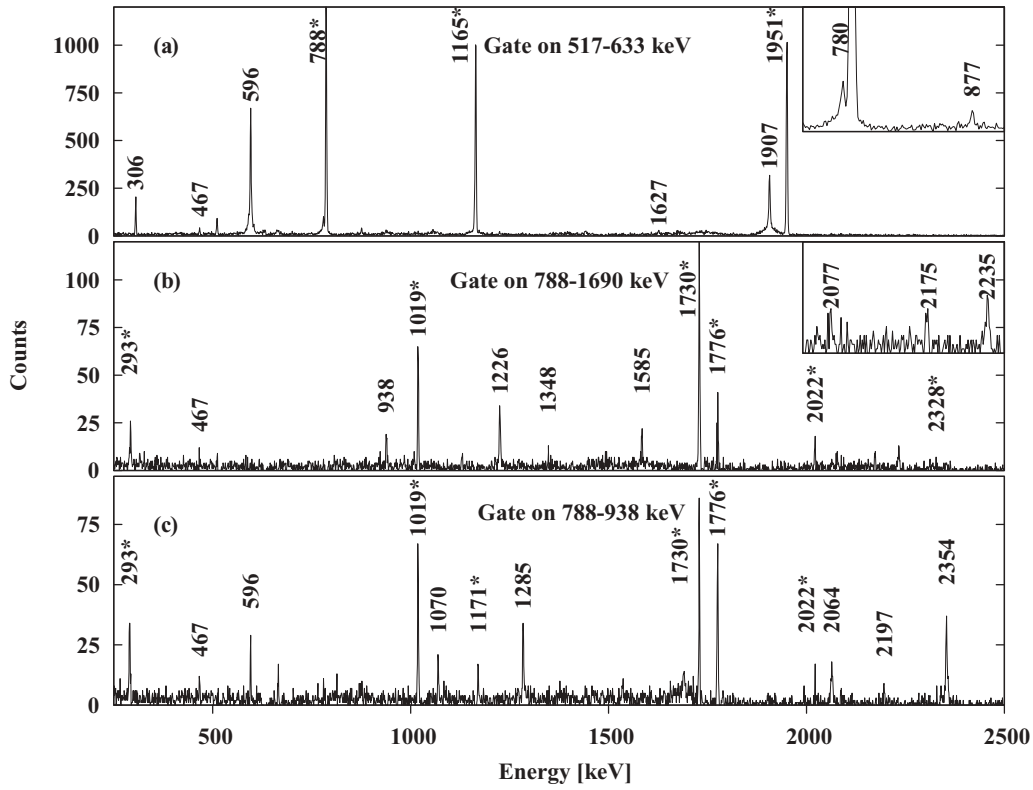

FIG. 1. Background-subtracted coincidence spectra obtained from the symmetric γ-γ-γ cube gated by (a) 517- and 633-keV γ rays, (b) 788- and 1690-keV γ rays, and (c) 788- and 938-keV γ rays. Less-intense peaks are shown in the inset and previously known γ rays are marked with a star (*).

The transitions deexciting these states, being emitted from stopped nuclei in the thick target, show up as narrow peaks in our spectra. All other transitions showed Doppler-broadened line shapes owing to the recoils slowing down in the target; however, it was observed that almost all γ rays presented unshifted components that were observed as narrow peaks in the symmetric matrices. This was attributable to the fact that several states located at high excitation energy have rather long lifetimes (see Sec. III) and a sizable number of deexcitations occur in already stopped ^{36}Cl nuclei. The level scheme has been constructed based mainly on the observed γ-γ coincidences in symmetric matrices. Typical examples of double-gated γ-ray spectra are reported in Fig. 1. A few γ-ray lines, deexciting the highest-lying levels, showed no stopped component. They were identified in spectra corresponding to the detectors placed at 90° after a coincidence relationship was required with some of the previously identified transitions from states at lower excitation energy.

The presence of Doppler-broadened shapes did not allow to extract reliable information on the intensity of the observed γ rays when gating on lower-lying transitions in the symmetric matrices. However, by gating on the stopped components of transitions lying above the levels of interest, only the stopped component of the subsequent transitions lying below is observed and, thus, branching ratios could be determined for most excited states. Information about the relative γ intensities was obtained from the asymmetric matrices by narrow gating on low-lying transitions on the axis where all detectors are added together and integrating on the broadened lines. To minimize the angular distribution effects, matrices at 60° and 120° were used.

To obtain information on the multipolarity and mixing ratio of the observed γ-ray transitions, angular distribution analysis was performed, using efficiency-corrected γ-ray intensities, $I_\gamma(\theta)$, obtained from the asymmetric matrices by gating on the axis where all detectors are included. The experimental angular distributions were fitted using standard Legendre polynomials $P_{2,4}(\cos\theta)$ with free angular distribution coefficients $A_{2,4}$. The angular distributions were also analyzed considering as free parameters the mixing ratio δ and the degree of alignment σ, with Gaussian functions describing the distributions of the m-state populations [19]. In Fig. 2 the angular distribution results are shown for three transitions which are representative of a mixed dipole + quadrupole transition (788 keV), a stretched quadrupole transition (1226 keV), and a stretched dipole transition (596 keV).

For low-intensity transitions, when angular distribution measurement was unfeasible, multipolarity information has been obtained from the angular distribution ratio $R_{\rm ADO}$ defined as Refs. [20,21]: $R_{\rm ADO} = [I_\gamma(34°) + I_\gamma(146°)]/2I_\gamma(90°)$.

In the GASP geometry reference values of $R_{\rm ADO}$ are 0.8 and 1.4 for stretched dipole and stretched quadrupole transitions, respectively. However, for transitions with mixed character, the situation is less straightforward because $R_{\rm ADO}$ depends on the value and sign of the mixing ratio δ [22].

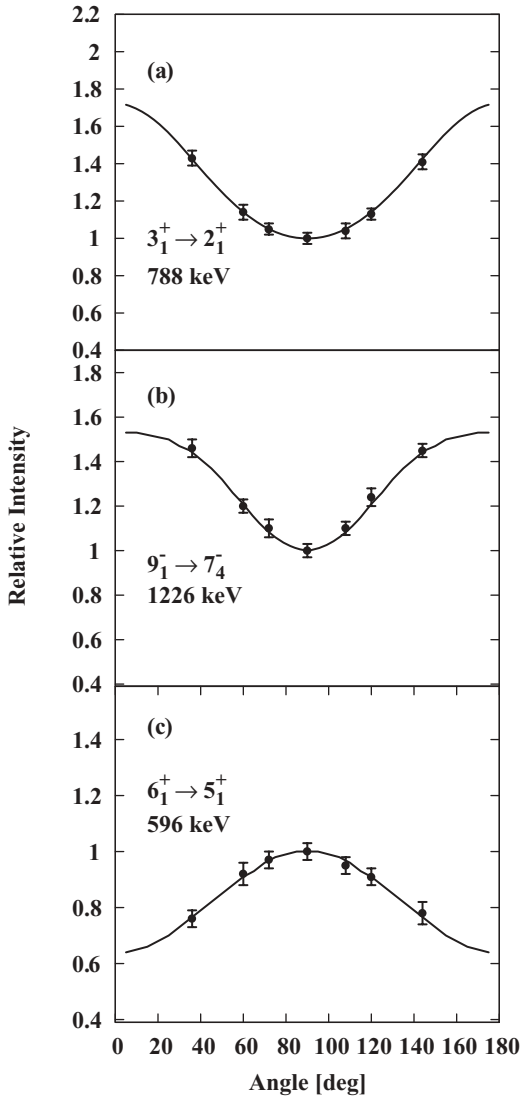

FIG. 2. Angular distribution results for the 788-, 1226-, and 596-keV transitions. The A_2, A_4 coefficients and the mixing ratio δ resulting from the fit are given in Table I.

III. EXPERIMENTAL RESULTS

A. Level scheme of ^{36}Cl

In the present work the level scheme of ^{36}Cl has been considerably extended at larger spins and excitation energies with respect to previous studies. Twenty new states, ten of positive parity and ten of negative parity, and 62 new γ-ray transitions, have been added. The results are summarized in Fig. 3 and Table I. The level scheme has been constructed on the basis of coincidence relationships in spectra created with appropriate gates on the symmetric γ-γ matrices. Spins for the new levels have been assigned based on measured γ-ray angular distributions while parities were inferred from determined lifetimes. The common assumption, for fusion-evaporation reactions, of assigning increasing angular momentum when increasing the excitation energy of the states, has been applied unless the deexcitation pattern proved contrary. All new stretched quadrupole transitions were assigned as $E2$. This assignment is supported by the lifetime measurements (see next section), as the $M2$ multipolarity would correspond to groundless transition strengths, much higher than the upper limit of 3 W.u. expected for this mass region [23]. The same argument has been used to rule out the $E1 + M2$ assignment in some cases of mixed dipole + quadrupole transitions.

The most intense transition in the level scheme is the well-known 788 keV from the 3^+ state to the 2^+ ground state. Its angular distribution, shown in Fig. 2(a), indicates a mixed $M1 + E2$ character with the mixing ratio $\delta = +0.50 \pm 0.03$. This agrees with the previous work by Yousef *et al.* [3], where a larger mixing ratio was proposed. The $M1/E2$ character of the 788-keV transition is clearly confirmed by our data and therefore the spin/parity of $J^\pi = 3^+$ for the 788-keV state.

Many previously known transitions in ^{36}Cl have been observed in our experiment. Their placement in the level scheme as well as the spin-parity assignment of the known states has been largely confirmed. Exceptions are discussed below together with the newly observed transitions.

1. Positive-parity states

The positive-parity states known from previous studies in ^{36}Cl are low-lying states of low spins 1^+, 2^+, and 3^+, as well as a state at 5314 keV and $J^\pi = 7^+$, which decays by two transitions of 1019 and 2795 keV to the 6^- and 5^- states at 4295 and 2519 keV, respectively [12–14].

In the present work three transitions of 1907, 2197, and 2489 keV were found to deexcite a state at an excitation energy of 5008 keV. Its 5^+ spin-parity assignment is based on the angular distribution analysis of the 1907-keV transition to the known 4^- state at 3101 keV. The assignment is supported by the presence of an $E2$ feeding transition of 306 keV from the known 7^+ state at 5314 keV. Note that in the neighboring ^{34}Cl isotope a 5^+ state is located at a similar energy of 4824 keV and decays in a similar way to the lower-lying 4^- and 5^- states, as well as to the 3^+ state. In the case of ^{36}Cl the decay to the 3^+ state at 788 keV could not be observed because the corresponding transition energy of 4219 keV was outside the energy range of the electronics used in this experiment.

In the work of Warburton *et al.* [24] a $J = 8$ state was proposed at 5781 keV deexciting to the 7^+ state by a 467-keV transition observed in coincidence with the 1019-keV ($7^+ \rightarrow 6^-$) and 2795-keV ($7^+ \rightarrow 5^-$) γ rays. We could not confirm this assignment because, in our data, the 467-keV transition is not in coincidence with the 306-, 1019-, and 2795-keV γ rays. The 467-keV transition is, however, in coincidence with all the transitions below the 6^- state at 4847 keV and closely corresponds to the energy difference between the 7^+ and 6^- states. It is therefore placed deexcite the 7^+ state at 5314 keV. In ^{34}Cl, the corresponding $7^+ \rightarrow 6^-$ transition has an energy of 572 keV.

A new state identified at 5604 keV was found to decay to the lower-lying 7^+ and 5^+ states via the dipole transitions of 290 and 596 keV, respectively. This state was assigned as the yrast 6^+ state. It also decays through weaker transitions to the known negative-parity 5^- state at 2519 keV and to two new negative-parity states also assigned as 5^- located at 4158 and 4728 keV.

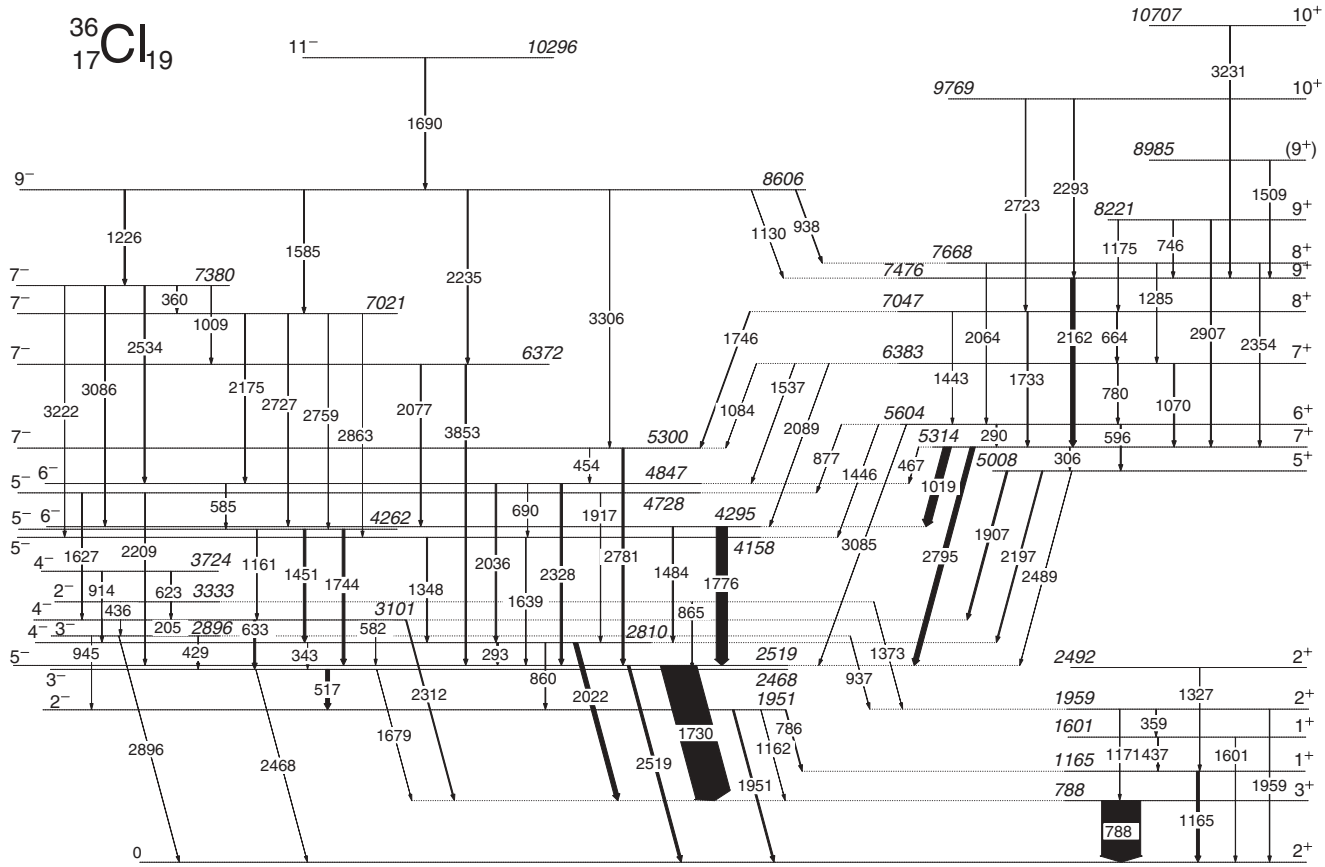

FIG. 3. Level scheme of ^{36}Cl based on the present work.

The state at 6383 keV excitation energy decays by the 1070-keV transition to the 7^+ state at 5314 keV and by the 780-keV transition to the 6^+ state at 5604 keV discussed above. The angular distribution coefficients and the mixing ratio established for the 780-keV transition leads unambiguously to a 7^+ assignment for the 6383-keV state. This assignment is also supported by the $R_{\rm ADO}$ value of the 1070-keV transition. The state decays also by weaker transitions to negative-parity states.

A new state was identified at 7047 keV excitation energy which decays toward the two lower-lying 7^+ states and the 6^+ state. The angular distribution data for the 664-keV transition to the 7^+ state at 6383 keV indicate spin value $J = 8$. The positive parity is supported by the presence of the 1443-keV transition toward the 6^+ state. The state at an excitation energy of 7668 keV has been assigned as the second 8^+ state, based on the 2064-keV $E2$ decaying transition to the 6^+ state.

Another new positive-parity state is located at 7476 keV. This state decays only through a 2162-keV transition to the 7^+ level at 5314 keV. The angular distribution coefficients and the ADO ratio of this transition are typical for a stretched quadrupole transition and therefore a spin parity of 9^+ is proposed for the state. Our assignment is supported by the presence in the neighbor odd-odd nucleus ^{34}Cl of a 9^+ state that was identified [25] at about the same excitation energy and decaying with an high-energy $E2$ transition to the lower 7^+ state. Spin-parity 9^+ is proposed also to the new state at 8221 keV, which decays through a 2907-keV, $E2$ transition to the known 7^+ state at 5314 keV. A new level at 8985 keV is tentatively assigned as the (9^+) state, based on the measured $R_{\rm ADO}$ value of the 1509-keV transition to the 9^+ state at 7476 keV.

The state located at 9769 keV was assigned as the yrast 10^+ state as it decays through the 2723-keV $E2$ and the 2293-keV mixed $M1 + E2$ transitions toward the yrast 8^+ and 9^+ states, respectively. The 10 707-keV state is the highest-energy state identified in ^{36}Cl and a spin-parity $J^\pi = 10^+$ was assigned to it on the basis of its decay via the 3231-keV mixed $M1 + E2$ transition to the yrast 9^+ state.

2. *Negative-parity states*

Negative-parity states with spin values between 2^- and 6^- have been previously reported in ^{36}Cl [12–14]. The highest spin state 6^- was known at an energy of 4295 keV.

In the present experiment spin-parity 6^- is proposed to the state at 4847 keV because it decays through the 2328-keV $M1 + E2$ and 2036-keV $E2$ transitions to the known states 5^- at 2519 keV and 4^- at 2811 keV, respectively. The 6^- state populates through a 585-keV transition of a mixed $M1 + E2$ character a new level at 4262 keV excitation energy, assigned as a 5^- state. The same spin and parity were assigned to a new state at 4158 keV, populated, among others, by a dipole transition of 690 keV from the 6^- state at 4847 keV and deexcited by a mixed $M1 + E2$ transition of 1348 keV to the previously known 4^- state at 2811 keV. Another 5^-

TABLE I. Initial state energies, spins and parities for initial and final states and transition energies in ^{36}Cl, as well as angular distribution coefficients, mixing ratios (δ), ADO ratios, relative intensities and multipolarities. Previously known states are marked with a star ($*$).

E_i (keV)	$J_i^\pi \rightarrow J_f^\pi$	E_γ (keV)	A_2	A_4	δ	R_{ADO}	I_γ^{rel}	γ_{mult}
788.4*	$3^+ \rightarrow 2^+$	788.4 (6)	0.38(11)	0.04(2)	0.50(3)	1.42(6)	1000(40)	$M1+E2$[a,b]
1164.7*	$1^+ \rightarrow 2^+$	1164.7 (6)				0.87(21)	75(4)	$M1+E2$[a]
1601.1*	$1^+ \rightarrow 1^+$	436.5 (5)					2.9(6)	
	2^+	1601.1 (6)					6.7(7)	
1951.0*	$2^- \rightarrow 1^+$	786.4 (5)					24.2(9)	
	3^+	1162.4 (5)					5.3(3)	
	2^+	1951.0 (3)					44(3)	
1959.2*	$2^+ \rightarrow 1^+$	358.5 (5)					0.2(1)	
	3^+	1171.0 (4)					0.4(1)	
	2^+	1959.2 (4)					11.9(3)	
2467.9*	$3^- \rightarrow 2^-$	517.3 (3)	−0.21(6)	0.001(1)	0.05(3)	0.80(6)	86(4)	$M1+E2$[a,b]
	3^+	1679.4 (2)					1.2(2)	
	2^+	2467.9 (3)					1.2(1)	
2492.3*	$2^+ \rightarrow 1^+$	1327.3 (4)					7.8(4)	
2518.6*	$5^- \rightarrow 3^+$	1729.9 (2)	0.27(7)	−0.13(3)	−0.07(2)	1.41(6)	903(22)	$M2+E3$[a,b]
	2^+	2518.6 (5)	0.54(12)	0.06(3)		1.58(11)	67(4)	$E3$ [a,b]
2810.5*	$4^- \rightarrow 5^-$	292.5 (5)	−0.12(3)	0.0001(1)	−0.01(1)	0.86(6)	44(2)	$M1(+E2)$[a,b]
	3^-	342.8 (3)					3.3(4)	
	2^-	859.7 (1)	0.32(11)	−0.09(4)		1.40(4)	19.7(5)	$E2$
	3^+	2021.9 (3)	−0.37(8)	−0.001(1)	−0.07(4)	0.69(3)	113(3)	$E1+M2$[a,b]
2896.4*	$3^- \rightarrow 3^-$	428.5 (2)					0.3(2)	
	2^+	937.2 (3)					10.9(6)	
	2^-	945.3 (1)					3.1(4)	
	2^+	2895.6 (6)					7.3(7)	
3100.7*	$4^- \rightarrow 3^-$	204.5 (4)					1.1(2)	
	5^-	582.4 (5)					0.9(2)	
	3^-	633.1 (2)	−0.29(11)	0.0002(2)	−0.02(1)	0.73(4)	52(2)	$M1+E2$[a,b]
	3^+	2311.9 (4)					27.6(9)	
3332.8*	$2^- \rightarrow 3^-$	436.4 (4)					0.7(2)	
	3^-	864.5 (6)					0.5(2)	
	2^+	1372.9 (3)					1.6(4)	
3723.8*	$4^- \rightarrow 4^-$	623.1 (2)					2.6(3)	
	4^-	913.8 (4)					14.2(9)	
4157.9	$5^- \rightarrow 4^-$	1347.5 (3)	−0.39(13)	0.003(2)	−0.11(5)	0.70(4)	28(2)	$M1+E2$
	5^-	1639.3 (3)					10(1)	
4261.9	$5^- \rightarrow 4^-$	1161.3 (2)					10.5(8)	
	4^-	1451.4 (1)					64(8)	
	5^-	1743.5 (3)					79(4)	
4294.6*	$6^- \rightarrow 4^-$	1484.1 (1)	0.31(8)	−0.08(3)		1.41(5)	32(3)	$E2$[a,b]
	5^-	1776.1 (2)	0.65(17)	0.12(4)	0.86(20)	1.79(18)	287(6)	$M1+E2$[a,b]
4727.5	$5^- \rightarrow 4^-$	1626.8 (2)					4.3(3)	
	4^-	1917.0 (4)	−0.41(14)	0.003(1)	−0.13(5)	0.73(4)	8.7(7)	$M1^-E2$
	5^-	2208.6 (2)					16(2)	
4846.8	$6^- \rightarrow 5^-$	585.4 (2)	−0.51(8)	0.01(1)	−0.21(5)	0.63(21)	2.1(1)	$M1+E2$
	5^-	689.5 (3)				0.82(18)	1.3(2)	$M1$
	4^-	2036.2 (3)	0.31(6)	−0.08(2)		1.43(4)	37(3)	$E2$
	5^-	2328.2 (3)	−0.73(17)	0.03(2)	−0.46(13)	0.46(12)	57(2)	$M1+E2$
5007.8	$5^+ \rightarrow 4^-$	1907.1 (6)	−0.34(13)	0.001(1)	−0.07(3)	0.75(7)	47(2)	$E1^-$M2
	4^-	2197.1 (6)					32(1)	
	5^-	2489.2 (6)					4.9(3)	
5300.1	$7^- \rightarrow 6^-$	454.0 (2)				0.87(5)	4.8(9)	$M1$
	5^-	2781.1 (3)	0.31(4)	−0.07(3)		1.41(3)	55 (4)	$E2$
5313.7*	$7^+ \rightarrow 5^+$	306.0 (2)	0.34(9)	−0.09(3)		1.42(3)	1.6(4)	$E2$
	6^-	467.3(3)	−0.29(8)	0.0006(5)	−0.06(3)	0.76(4)	12 (1)	$E1+M2$
	6^-	1019.2 (1)	−0.27(6)	0.0003(2)	−0.04(3)	0.78(4)	205(4)	$E1^-$M2[a,b]
	5^-	2794.7 (4)	0.51(7)	0.05(3)	0.26(12)	1.62(5)	127(6)	$M2+E3$[a,b]

TABLE I. *(Continued.)*

E_i (keV)	$J_i^\pi \rightarrow J_f^\pi$	E_γ (keV)	A_2	A_4	δ	R_{ADO}	I_γ^{rel}	γ_{mult}
5604.1	$6^+ \rightarrow 7^+$	289.9 (3)				0.82(5)	22 (1)	$M1$
	5^+	596.3 (4)	−0.31(4)			0.73(4)	28 (2)	$M1$
	5^-	876.5 (4)				0.75(10)	7.0(4)	$E1$
	5^-	1446.0 (4)					2.5(4)	
	5^-	3084.6 (8)	−0.62(17)	0.02(3)	−0.32(12)	0.55(7)	7.1(5)	$E1+M2$
6372.0	$7^- \rightarrow 6^-$	2077.4 (5)					26(1)	
	5^-	3852.9 (9)				1.43(4)	36(3)	$E2$
6383.4	$7^+ \rightarrow 6^+$	779.5 (9)	−0.47(11)	0.007(3)	−0.19(7)	0.62(6)	13(1)	$M1+E2$
	7^+	1070.1 (5)	0.34(13)			1.42(3)	33(3)	$M1$
	7^-	1084.0 (3)					4.5(9)	
	6^-	1536.6 (6)				0.83(10)	8.3(7)	$E1$
	6^-	2088.8 (6)					5.6(4)	
7021.3	$7^- \rightarrow 6^-$	2174.8 (4)				0.75(4)	26(1)	$M1$
	6^-	2726.8 (9)					12.3(7)	
	5^-	2759.4 (3)				1.42(4)	7.3(7)	$E2$
	5^-	2863.4 (4)					3.3(6)	
7046.9	$8^+ \rightarrow 7^+$	663.5 (3)	−0.31(9)			0.76(5)	18.3(8)	$M1$
	6^+	1442.9 (5)					3.7(4)	
	7^+	1733.2 (6)					28.1(7)	
	7^-	1746.4 (3)					21.0(6)	
7380.3	$7^- \rightarrow 7^-$	359.5 (4)					1.6(2)	
	7^-	1008.6 (3)					13.5(3)	
	6^-	2533.6 (2)					32(2)	
	6^-	3086.4 (4)					11(1)	
	5^-	3222.2 (5)					7.7(6)	
7475.7	$9^+ \rightarrow 7^+$	2162.4 (6)	0.31(6)	−0.08(4)		1.42(3)	114(5)	$E2$
7667.9	$8^+ \rightarrow 7^+$	1284.5 (6)				0.69(9)	6.8(4)	$M1$
	6^+	2064.2 (4)				1.38(5)	5.4(2)	$E2$
	7^+	2354.0 (8)	−0.16(8)	0.002(1)	0.03(2)	0.87(4)	13.9(8)	$M1+E2$
8221.3	$9^+ \rightarrow 9^+$	745.6 (3)					11.5(4)	
	8^+	1174.7 (4)	−0.68(11)	0.03(2)	−0.31(12)	0.51(10)	11.9(5)	$M1+E2$
	7^+	2906.8 (7)	0.32(7)	−0.08(3)		1.44(4)	27.4(3)	$E2$
8606.0	$9^- \rightarrow 8^+$	938.4 (6)				0.75(10)	18.5(9)	$E1$
	9^+	1130.4 (7)					7.3(8)	
	7^-	1225.7 (3)	0.32(4)	−0.08(3)		1.40(3)	37(2)	$E2$
	7^-	1584.7 (4)	0.28(11)	−0.06(4)		1.40(9)	25(1)	$E2$
	7^-	2234.7 (2)				1.43(4)	27(3)	$E2$
	7^-	3306.3 (4)					4.0(7)	
8984.5	$(9^+) \rightarrow 9^+$	1508.8 (3)				1.40(8)	12.3(3)	
9769.1	$10^+ \rightarrow 9^+$	2293.0 (5)	−0.89(21)	0.08(4)	−0.73(21)	0.33(11)	19.9(8)	$M1+E2$
	8^+	2722.6 (4)	0.30(7)	−0.06(4)		1.41(3)	15.0(1)	$E2$
10 296.2	$11^- \rightarrow 9^-$	1690.3 (3)	0.31(8)	−0.07(4)		1.43(4)	26(2)	$E2$
10 707.1	$10^+ \rightarrow 9^+$	3231.4 (6)	−0.72(15)	0.029(8)	−0.30(15)	0.50(12)	9.6(5)	$M1+E2$

[a]Multipolarity previously known.
[b]Previously assigned multipolarity is confirmed.

state was identified at 4728 keV, the spin/parity assignment being supported by its decay through the 1917-keV $M1+E2$ transition to the known 4^- state at 2811 keV.

Spin-parity $J^\pi = 7^-$ was assigned to the four states at excitation energies of 5300, 6372, 7021, and 7380 keV, because they deexcite by $E2$ transitions to 5^- states. A new negative-parity state was identified at 8606 keV and assigned $J^\pi = 9^-$ based on the deexciting $E2$ transitions to the 7^- states. This state populates also the 8^+ and 9^+ positive-parity states through dipole transitions.

The 1690-keV transition depopulating the state at 10 296-keV shows an angular distribution typical of a quadrupole leading to $J^\pi = 11^-$ assignment to the state. This is the largest spin observed in our experiment.

B. Lifetime measurements

In previous studies lifetimes for the low-spin states in ^{36}Cl have been reported [13,14]. The state at 2519 keV excitation energy is an isomer with $T_{1/2} = 1.61(8)$ ns. Lifetimes in

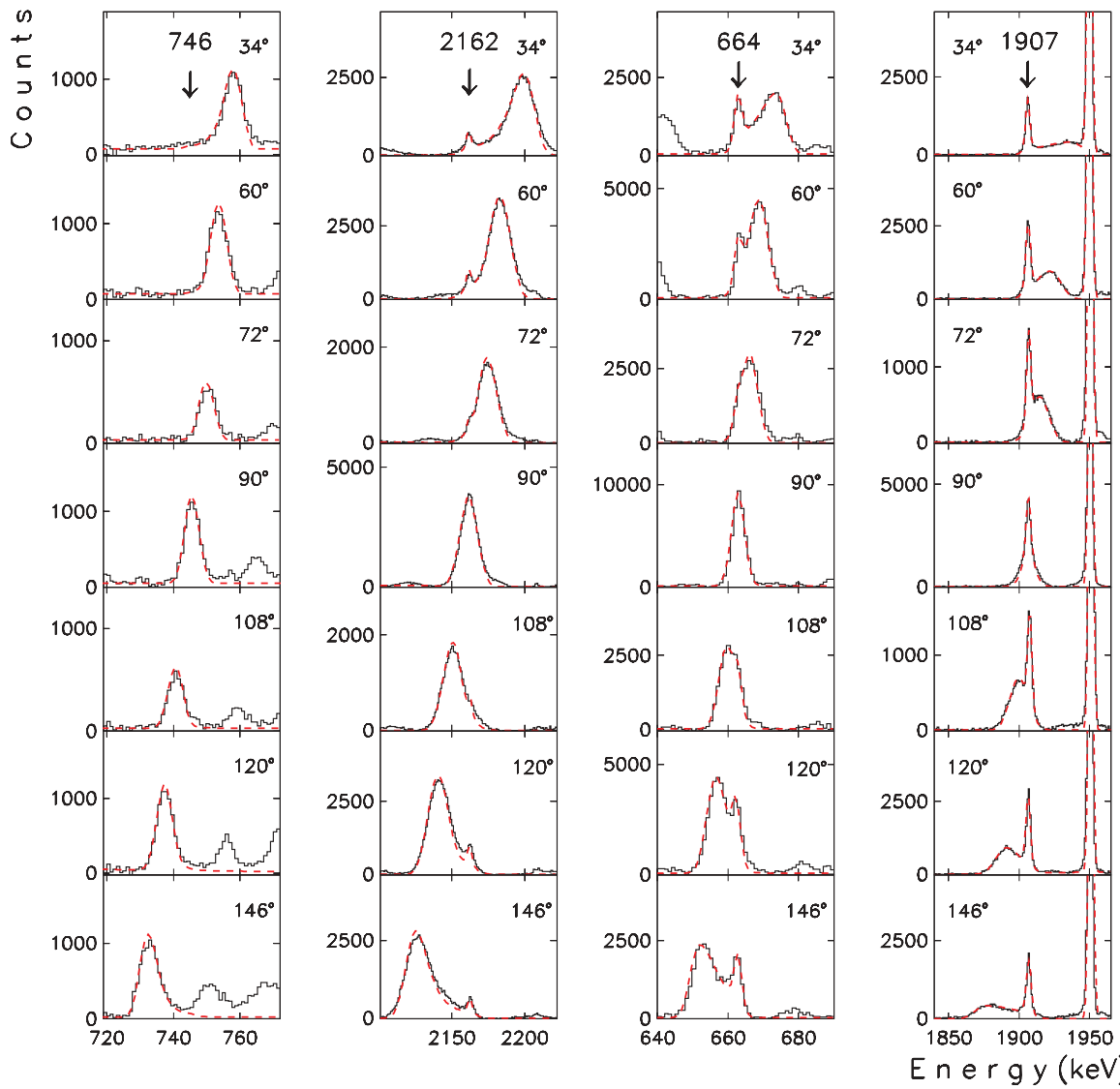

FIG. 4. (Color online) Experimental and calculated line shapes for the 746-, 2162-, 664-, and 1907-keV transitions deexciting the positive-parity states at 8221, 7476, 7047, and 5008 keV, respectively, in ^{36}Cl. The coincidence spectra were created with narrow gate on lower-lying transitions emitted from stopped nuclei. The fitted DSAM spectra are shown in red dashed line.

the ps-range, $T_{1/2} = 14.7(10)$, 6.9(4), 1.87(21), 2.36(21), and 19.7(15) ps, were measured for the 788-, 1165-, 1951-, 2811-, and 5314-keV states, respectively. The other low-lying states have shorter lifetimes, in the fs range.

The data of the present experiment have been analyzed to obtain lifetime information by applying the Doppler shift attenuation method (DSAM). For this purpose spectra of interest were created from the asymmetric γ-γ matrices by gating on appropriate lower-lying transitions emitted from stopped nuclei. The spectra for all analyzed transitions were obtained by summing those gates that minimized the contents of contaminants in the energy region of interest.

The analysis has been performed using the LINE-SHAPE code [26], modified to allow, for each level, side populations from two independent levels. This was particularly important in the present case where many levels have a fraction of their population coming from longer-lived states. The slowing-down history of ^{36}Cl recoils in the target and backing was simulated using Monte Carlo techniques and a statistical distribution was created for the projection of the recoil velocity with respect to the direction of the detected γ ray. Moreover, the kinematic effects of the nucleon evaporation were included, as well as the finite solid angles of the detectors. For the description of the electronic and nuclear scattering the Ziegler [27,28] stopping powers have been adopted. To estimate the systematic error introduced by the stopping powers, several intense transitions have been also analyzed using the Northcliffe-Schilling parametrization [29] corrected for atomic shell effects [30]. The lifetimes derived using the two parametrizations were found consistent within 10%. We assigned therefore a conservative systematic uncertainty of 12% owing to the stopping-power calculation.

DSAM analysis has been performed for all new states in ^{36}Cl. The obtained information for the higher levels was used in the analysis of the lower states. At each level the intensity balance of feeding and decaying transitions was calculated using the γ intensities of Table I, making it possible to establish the amount of the fast side feeding from unobserved transitions. The transitions of 3231, 2293, 1509, and 1627 keV deexiting the states at 10 707, 9769, 8985, and 4728 keV, respectively, showed full Doppler shift in spectra registered at backward and forward detectors. An upper limit of $T_{1/2} <$ 0.05 ps has been assigned for these levels. No clean spectra could be obtained for transitions deexciting the levels 7^-_3 7021 keV and 7^-_4 7380 keV, the presence of many contaminants preventing lifetime determination. From line-shape analysis, lifetimes have been derived for 14 new levels in ^{36}Cl, as well as for the 4295-keV state previously known without measured lifetime. Examples of experimental line shapes at different angles and the corresponding fits are illustrated in Figs. 4 and 5 for transitions deexciting states of positive and negative parity, respectively. Lifetimes determined by the present DSAM analysis are collected in Table II.

IV. COMPARISON WITH SHELL-MODEL PREDICTIONS

In ^{36}Cl the valence particles occupy the *sd* shell. However, having this nucleus only one neutron hole and three proton holes with respect to the $N = 20$ and $Z = 20$ shell closures, cross shell excitations to the *fp* orbitals become important at relatively low excitation energies. To interpret the properties of ^{36}Cl, we have performed shell-model calculations using different interactions and model spaces.

The calculations have been done with the shell-model code ANTOINE [31]. In a first stage, positive-parity states have been calculated in the *sd* valence space using the USD effective

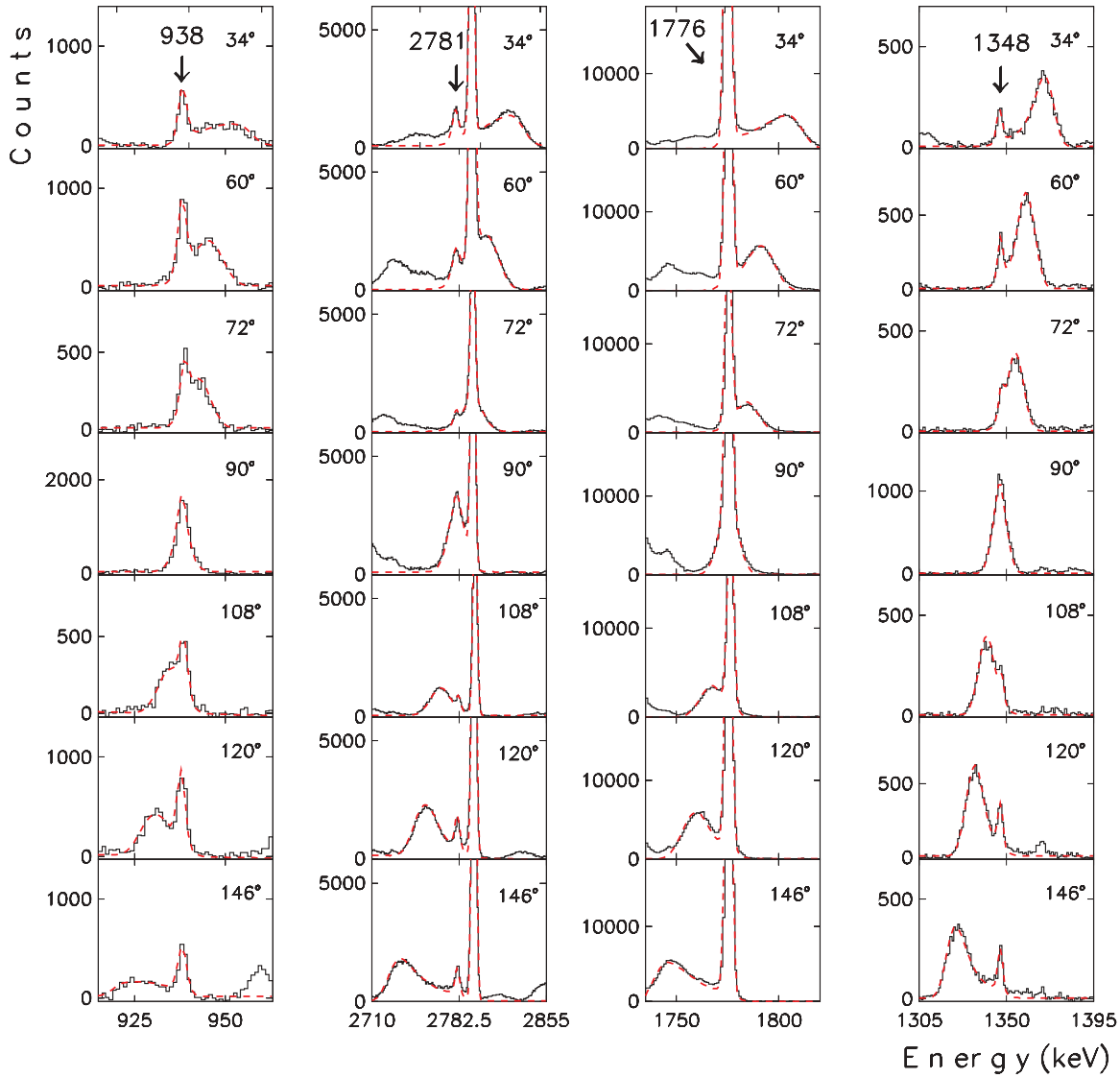

FIG. 5. (Color online) Experimental and calculated line shapes for the 938-, 2781-, 1776-, and 1348-keV transitions deexciting the negative-parity states at 8606, 5300, 4295, and 4158 keV, respectively, in ^{36}Cl. The coincidence spectra were created with narrow gate on lower-lying transitions emitted from stopped nuclei. The fitted DSAM spectra are shown in red dashed line.

TABLE II. Half-lives determined in the present work for excited states in ^{36}Cl. Previously known state is marked with a star (∗).

E_x (keV)	J^π	$T_{1/2}$ (ps)
4157.9	5_2^-	0.13(4)
4261.9	5_3^-	0.22(8)
4294.6*	6_1^-	0.23(5)
4846.8	6_2^-	0.17(4)
5007.8	5_1^+	0.42(8)
5300.1	7_1^-	0.16(5)
5604.1	6_1^+	0.62(14)
6372.0	7_2^-	0.13(3)
6383.4	7_2^+	0.24(5)
7046.9	8_1^+	0.34(6)
7475.7	9_1^+	0.18(3)
7667.9	8_2^+	0.07(2)
8221.3	9_2^+	0.09(2)
8606.0	9_1^-	0.55(9)
10 296.2	11_1^-	0.24(4)

interaction [32]. The comparison between the experimental states and the calculated ones is shown in Fig. 6. Only the low-spin states (i.e., 1^+, 2^+, and 3^+) are found to be in good agreement with the shell-model predictions. The wave function of the 2^+ ground state and the 1^+ and 3^+ yrast states are dominated by the $\nu d_{3/2}^{-1}\pi d_{3/2}^{1}$ configuration, while the second 1^+ state has a $\nu d_{3/2}^{-1}\pi s_{1/2}^{-1}$ configuration. The higher-spin states are predicted at much higher energies than those observed experimentally. This indicates that the restricted sd model space is not good enough for states with $J > 3$, for which particle-hole excitations to the fp shell contribute to the wave functions. We have therefore extended our model space to include these excitations and to calculate the negative-parity states. For this purpose we have used a new interaction developed by Bouhelal *et al.* [33], the PSDPF interaction. This interaction considers the full $psdpf$ model space with a ^{4}He core. Negative-parity states of $1\hbar w$ nature can be obtained by allowing one nucleon jump between major shells. The results for positive- and negative-parity states are reported in Figs. 6 and 7, respectively. The results for the positive-parity states are similar to those obtained with the USD interaction, with the 5^+ state predicted to be too high in excitation energy. Negative-parity states are described satisfactorily up to the 7^- states.

From the analysis of the wave functions, it results that for $J^\pi \geqslant 9^-$ the leading configuration has holes in the $d_{5/2}$ shell. With the restriction of only one intruder excitation to the fp shell, these holes are needed to construct such angular momenta. More than one particle-hole excitation across the shell gap introduces spuriousness owing to the center-of-mass motion. To avoid this problem and to allow more than one particle-hole excitation to the fp shell, we have adopted the model space spanned by the $s_{1/2}$, $d_{3/2}$, $f_{7/2}$, and $p_{3/2}$ orbits. The interaction in this model space is the $sdfp$ interaction [34]. The results for the positive-parity states are also shown in Fig. 6. Here, not only the low-spin,

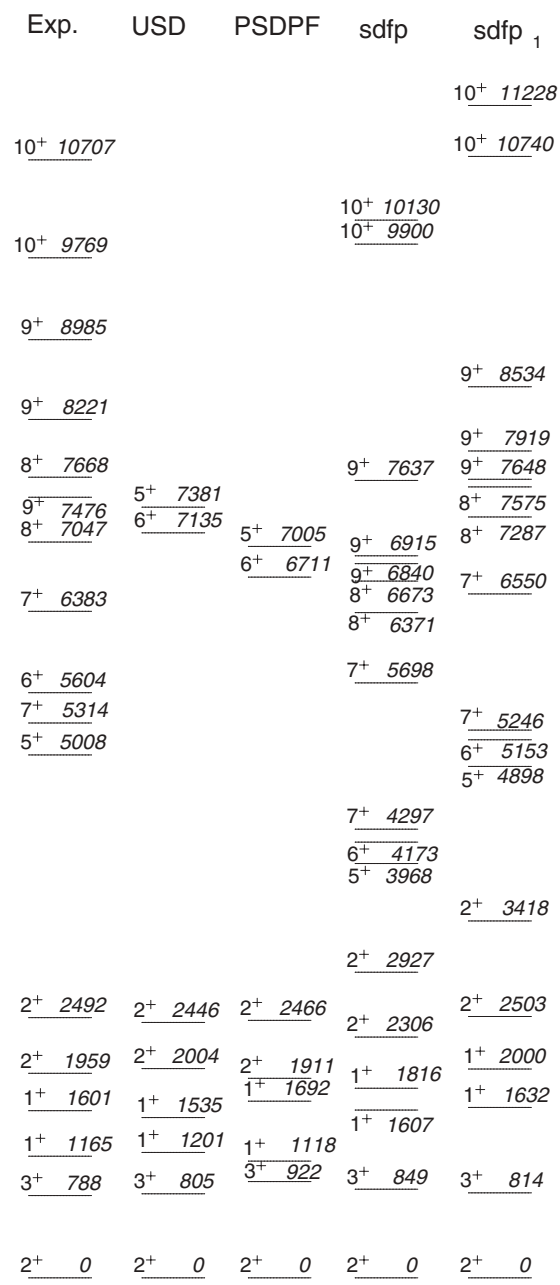

FIG. 6. Positive-parity states of ^{36}Cl observed in the present experiment compared with shell-model calculations using the code ANTOINE with different model spaces and interactions.

positive-parity states are close to the observed ones but also the higher-spin states are in good agreement with the data. The calculations indicate that the wave function configuration of the states with $J^\pi \geqslant 5^+$ involve two particle-hole intruder excitations to the fp shell. This is consistent with the decay pattern: The 5^+ state decays to the negative-parity states, which involve one particle-hole excitation, instead of decaying to the 3^+ where a pure sd configuration is predicted. However, the excitation energy of the 5^+ state is predicted 1 MeV lower that the experimental value. A similar feature was previously noticed in Ref. [35] when the same effective interaction was used in the description of ^{37}Cl. In this reference it was

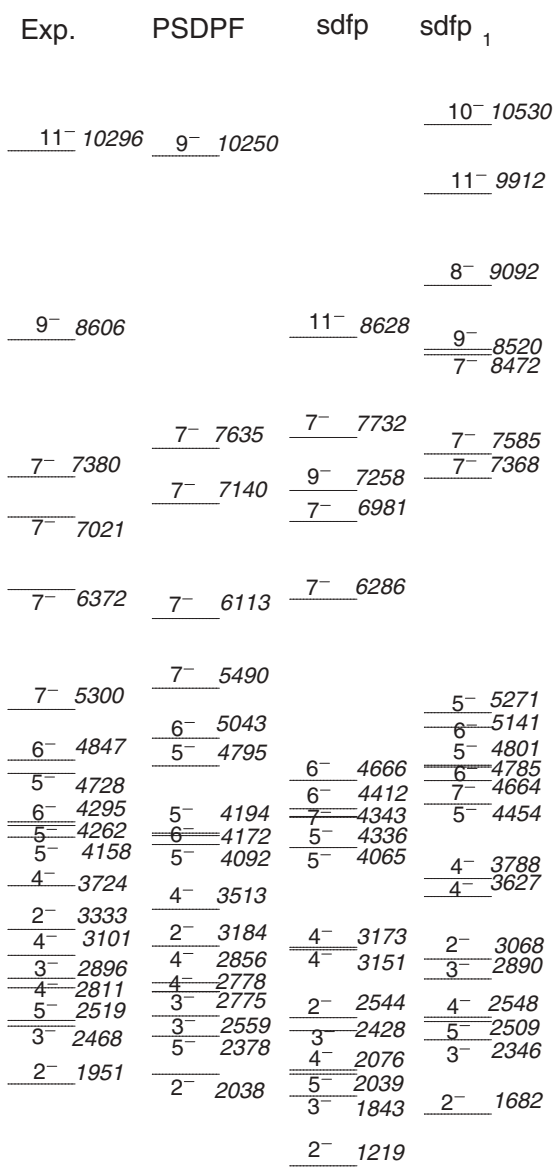

FIG. 7. Negative-parity states of ^{36}Cl observed in the present experiment compared with shell-model calculations using the code ANTOINE with different model spaces and interactions.

pointed out that to have better reproduction of the experimental findings, an increase by 500 keV in the single-particle energy of the $f_{7/2}$ orbital was necessary. We have therefore performed shell-model calculations with this modification. The new results ($sdfp_1$) are presented in Fig. 6, where it can be seen that the agreement between experimental data and shell-model predictions improves significantly. The configuration of the 5^+ and 7^+ yrast states involves the excitation of both a proton and a neutron into the fp shell, while the excitation of two neutrons into fp shell dominates the wave function of the yrast 9^+ state.

The results for the negative-parity states with both the $sdfp$ and the $sdfp_1$ interactions are reported in Fig. 7. Here the agreement between experimental data and shell-model prediction is quite satisfactory. For the low-spin states the $sdfp_1$ results are again better than those obtained without the modification of the $f_{7/2}$ single-particle energy. The yrast states' wave functions are dominated by the excitation of one neutron to the $f_{7/2}$ orbital and by a regular filling of the proton sd orbitals. Non-yrast states differ mainly on the proton orbital occupation, where the excitation from the $s_{1/2}$ to the $d_{3/2}$ constitutes the largest component, and the odd neutron occupies the $f_{7/2}$ shell. For high-spin states with $J^\pi \geqslant 9^-$ the excitation of two neutrons and a proton to the fp shell becomes dominant. As seen in Fig. 7, the $sdfp_1$ calculations predict the occurrence of the first 8^- and 10^- states above the 9^- and 11^- states, respectively. These states were not observed experimentally, being most probably more weakly populated as they are non-yrast, in accordance with calculations. We note that the better description of the states with $J^\pi \geqslant 9^-$, with respect to the PSDPF results is attributable to the fact that the promotion of three nucleons from the $s_{1/2}$ and $d_{3/2}$ to the fp shell is energetically favored with respect to a configuration that involves only one particle in the fp shell and particle-hole excitations from the $d_{5/2}$. Unfortunately, calculations that allow all these degrees of freedom are not yet achievable.

Using the measured half-lives (from Ref. [14] and this work) the experimental $B(M1)$ and $B(E2)$ reduced transition probabilities have been obtained. For $M1+E2$ mixed transitions the mixing coefficients δ from Table I have been employed to estimate the corresponding partial lifetimes. For the 1165-keV transition from the first 1^+ state the value of $\delta = -0.32(6)$ from Ref. [14] was used.

The experimental reduced transition probabilities are compared in Tables III and IV with shell-model calculations for positive- and negative-parity states, respectively. The values derived using the $sdfp$ and $sdfp_1$ interactions were quite similar; therefore, only results of the $sdfp_1$ calculations were included in the tables.

As seen in Table III the USD and PSDPF calculations provide an overall good description of the reduced transition probabilities between positive-parity states of low spins. A marked discrepancy is obtained only for the $B(E2)$ of the 1165-keV transition. We note that the ground-state magnetic moment, $\mu_{\rm exp}(2^+) = +1.285\,47(5)$ [14], is very well reproduced by calculations, $\mu_{\rm USD}(2^+) = +1.266$ and $\mu_{\rm PSDPF}(2^+) = +1.170$, giving strong support to the composition of the wave functions predicted by the corresponding interactions. However, a value of $\mu_{spdf_1}(2^+) = +0.746$, in worse agreement with the experimental magnetic moment, is calculated with the $spdf_1$ interaction which does not include the $d_{5/2}$ orbital. The predictions of the $spdf_1$ calculations are in a satisfactory accordance with experimental $B(M1)$ and $B(E2)$ values for transitions from both low- and high-spin states. The $E2$ transition strength between the yrast 9^+ and 7^+ states is, however, largely underestimated by the calculations. This is attributable to the different predicted underlying structure of the involved states, namely the excitation into the fp shell of a proton and a neutron for the 7_1^+ state and of two neutrons for the yrast 9^+ state. We note that for the 9_2^+ and 9_3^+ states the calculated configuration is dominated by a proton and a neutron in the fp shell, similar to that of the 7_1^+ state. If we consider an inversion of states, with the 9_1^+ and 9_2^+ observed states described by the 9_2^+ and 9_3^+ shell-model states, respectively, a good description of the experimental $B(E2)$

TABLE III. Experimental reduced transition probabilities $B(M1)$ and $B(E2)$ for positive-parity states in ^{36}Cl compared to shell-model calculations performed with the code ANTOINE using the USD, PSDPF, and $sdfp_1$ residual interactions (see text for details). In deriving the theoretical $B(M1)$ values free nucleon g factors have been used. The theoretical $B(E2)$ have been obtained using for the effective electric charges $e_\nu^{\rm eff} = 0.5e$ and $e_\pi^{\rm eff} = 1.5e$. The numbers in brackets for the $sdfp_1$ calculations are explained in the text.

$E_{\rm lev}^{\rm exp}$	$T_{1/2}^{\rm exp}$	J_i^π	J_f^π	$E_\gamma^{\rm exp}$	$BR^{\rm b}$	$B(M1)(\mu_N^2)$				$B(E2)(e^2\,{\rm fm}^4)$			
(keV)	(ps)			(keV)	(%)	Exp.	USD	PSDPF	$sdfp_1$	Exp.	USD	PSDPF	$sdfp_1$
788	14.7(10)[a]	3_1^+	2_1^+	788	100	0.004(1)	0.018	0.045	0.107	25(3)	36	34	27
1165	6.9(4)[a]	1_1^+	2_1^+	1165	100	0.003(1)	0.022	0.022	0.223	4(1)	50	29	34
1601	0.65(4)[a]	1_2^+	1_1^+	437	30(6)	0.219(46)	0.193	0.149	0.021				
			2_1^+	1601	70(8)	0.010(2)	0.004	0.030	0.009				
1959	0.044(2)[a]	2_2^+	1_2^+	359	1.6(2)	0.313(40)	0.733	0.594	1.242				
			3_1^+	1171	3.0(4)	0.017(2)	0.001	0.008	0.013				
			2_1^+	1959	95.4(25)	0.115(6)	0.137	0.082	0.029				
2492	0.040(9)[a]	2_3^+	2_2^+	533	9(2)[a]	0.587(191)	0.943	0.766	1.284				
			1_1^+	1327	82(4)[a]	0.346(80)	0.503	0.398	0.076				
			2_1^+	2492	9(3)[a]	0.006(2)	0.062	0.137	0.003				
5314	19.7(15)[a]	7_1^+	5_1^+	306	0.5(1)					53(13)			76
5604	0.62(14)[b]	6_1^+	7_1^+	290	33(6)	0.862(250)			0.826				
			5_1^+	596	42(5)	0.126(32)			0.384				
6383	0.24(5)[b]	7_2^+	6_1^+	780	21(2)	0.070(18)			0.048	60(40)			2
			7_1^+	1070	51(4)	0.068(17)			0.304				
7047	0.34(6)[b]	8_1^+	7_2^+	664	26(3)	0.102(22)			0.098				
			6_1^+	1443	5(1)					14(4)			12
			7_1^+	1733	40(4)	0.009(3)			0.051				
7476	0.18(3)[b]	9_1^+	7_1^+	2162	100					67(11)			1 [68]
7668	0.07(2)[b]	8_2^+	7_2^+	1285	26(2)	0.069(20)			0.077				
			6_1^+	2064	21(1)					45(14)			32
			7_1^+	2354	53(3)	0.023(9)			0.054	0.05(3)			0.51
8221	0.09(2)[b]	9_2^+	9_1^+	746	23(5)	0.240(72)			0.002				
			8_1^+	1175	23(4)	0.057(16)			0.002	57(42)			4
			7_1^+	2907	54(6)					16(5)			68 [7]

[a]Reference [14].
[b]Present study.

values for the $9^+ \to 7^+$ transitions could be obtained. This is shown in Table III where the corresponding calculated $B(E2)$ values under this assumption are given in brackets.

The predictions of the PSDPF and $sdfp_1$ calculations are in moderate agreement with experimental $B(M1)$ and $B(E2)$ values for the negative-parity states, as seen in Table IV. Note that the large $B(E2)$ value of the $11_1^- \to 9_1^-$ is reproduced by the $spdf_1$ calculations, in which the involved states are both described by the promotion of three nucleons into the fp shell. However, the PSDPF calculations, in which only one nucleon is excited in the fp shell, predict a much smaller $B(E2)$ value for this transition. In the $sdfp_1$ calculations the wave functions of the 7^- states involve one neutron excited in the fp shell, with the exception of the 7_3^- state where three nucleons are excited. A large $B(E2)$ value for the $9_1^- \to 7_3^-$ is correspondingly predicted, while experimentally the $B(E2)$ is largest for the $9_1^- \to 7_4^-$ transition. To reproduce the experimental findings one can consider again an inversion of states, with the 7_4^- observed state described by the calculated 7_3^- state, and the 7_2^- and 7_3^- experimental levels described by the 7_4^- and 7_2^- calculated states, respectively. The $B(E2)$ values corresponding to this inversion are given in brackets in Table IV and agree well with the experimental data.

V. SUMMARY

Excited states in the doubly odd ^{36}Cl nucleus have been populated via ^{24}Mg(^{14}N,$2p$) fusion evaporation reaction and their γ decay measured with the high-resolution 4π GASP array. A total of 20 new excited states deexciting through 62 new γ rays have been observed and are placed in the previously known level scheme of ^{36}Cl nucleus with proposed spins and parities. The spins and parities of the newly identified states have been adopted on the basis of angular distributions information of deexciting transitions and measured lifetimes. This work establishes the high-spin structure of ^{36}Cl up to the 10^+ state at 10 707 keV for positive parity and up to the 11^- state at 10 296 keV for negative parity. Experimental

TABLE IV. Experimental reduced transition probabilities B(M1) and B(E2) for negative-parity states in ^{36}Cl compared to shell-model calculations performed with the code ANTOINE using the PSDPF and $sdfp_1$ residual interactions (see text for details). In deriving the theoretical B(M1) values free nucleon g factors have been used. The theoretical B(E2) have been obtained using for the effective electric charges $e_\nu^{\rm eff} = 0.5e$ and $e_\pi^{\rm eff} = 1.5e$. The numbers in brackets for the $sdfp_1$ calculations are explained in the text.

$E_{\rm lev}^{\rm exp}$	$T_{1/2}^{\rm exp}$	J_i^π	J_f^π	$E_\gamma^{\rm exp}$	$BR^{\rm b}$	B(M1)(μ_N^2)			B(E2)(e^2 fm^4)		
(keV)	(ps)			(keV)	(%)	exp	PSDPF	$sdfp_1$	exp	PSDPF	$sdfp_1$
2468	0.97(10)[a]	3_1^-	2_1^-	517	97(4)	0.285(35)	0.134	0.118	$38(^{+59}_{-32})$	52	9
2811	2.36(21)[a]	4_1^-	5_1^-	293	25(1)	0.163(15)	0.003	0.055	$3(^{+8}_{-3})$	4	0.2
			3_1^-	343	1.8(2)	0.007(2)	0.073	0.004			
			2_1^-	860	10.9(3)				55(5)	3	21
2896	0.60(6)[a]	3_2^-	3_1^-	429	1.3(11)	0.011(9)	0.025	0.117			
			2_1^-	945	14(2)	0.011(2)	0.057	0.014			
3101	0.15(4)[a]	4_2^-	3_2^-	205	1.3(2)	0.400(125)	0.265	0.029			
			5_1^-	582	1.1(2)	0.015(5)	0.095	0.016			
			3_1^-	633	64(2)	0.664(178)	0.076	0.002	$9(^{+12}_{-7})$	6	5
3724	0.05(1)[a]	4_3^-	4_2^-	623	19(5)	0.633(211)	0.411	0.094			
			4_1^-	914	81(8)	0.858(195)	0.004	0.095			
4158	0.13(4)[b]	5_2^-	4_1^-	1348	74(6)	0.091(25)	0.050	0.0002	9(4)	74	0.02
			5_1^-	1639	26(4)	0.018(6)	0.052	0.006			
4262	0.22(8)[b]	5_3^-	4_2^-	1161	7(1)	0.008(3)	0.010	0.014			
			4_1^-	1451	42(1)	0.025(10)	0.014	0.005			
			5_1^-	1744	51(3)	0.017(6)	0.023	0.080			
4295	0.23(5)[b]	6_1^-	4_1^-	1484	10(1)				34(8)	0.002	0.002
			5_1^-	1776	90(2)	0.016(5)	0.011	0.066	53(20)	82	17
4847	0.17(4)[b]	6_2^-	5_3^-	585	2.2(1)	0.024(6)	0.0001	0.103	45(25)	0.02	3
			5_2^-	690	1.4(1)	0.010(3)	0.008	0.103			
			4_1^-	2036	38.1(10)				36(9)	2	44
			5_1^-	2328	58.3(15)	0.009(3)	0.013	0.058	5(3)	2	9
5300	0.16(5)[b]	7_1^-	6_2^-	454	8(2)	0.211(84)	0.046	0.029			
			5_1^-	2781	92(7)				20(6)	15	7
6372	0.13(3)[b]	7_2^-	6_1^-	2077	42(2)	0.014(3)	0.003	0.034			
			5_1^-	3853	58(4)				3(1)	3	6
8606	0.55(9)[b]	9_1^-	7_4^-	1226	32(1)				119(22)	13	9 [95]
			7_3^-	1585	21(1)				22(4)	1	95 [20]
			7_2^-	2235	22(2)				4(1)	12	20 [9]
			7_1^-	3306	3(1)				0.08(3)	12	0.2
10296	0.24(4)[b]	11_1^-	9_1^-	1690	100				171(29)	8	116

[a]Reference [14].
[b]Present study.

results have been interpreted in the framework of shell-model predictions using different model spaces and interactions, which make it possible to deduce the configurations of the observed states. By comparison with the data, it appears that the calculations in the reduced valence space $s_{1/2}d_{3/2}f_{7/2}p_{3/2}$, without limitations in the number of excitations, give better agreement than those in the full $psdpf$ space, where only one excitation across the shell gap is allowed, in particular at high spin. In fact, the data are consistent with the predictions that excitations of the odd proton and neutron to the fp main shell occur at relatively low spin in the positive-parity levels. Negative-parity states are predicted to have one neutron in the $f_{7/2}$ orbit at low spin and the proton in the sd shell, but the excitation of three particles (protons and neutrons) to the upper fp shell becomes relevant already at spin $J^\pi = 7^-$. In this regard, these new data that improve the level scheme of the odd-odd nucleus ^{36}Cl offer a good testing ground for effective interactions, model spaces, and related degrees of freedom, with the possibility of disentangling the relevant configurations at the different energy regimes.

ACKNOWLEDGMENTS

This work was carried out at the INFN Laboratori Nazionali di Legnaro (LNL), Italy. Authors are thankful to the XTU Tandem staff of LNL for delivering good-quality beam. S. Aydin thanks Sudeb Bhattacharya for very useful discussions during the preparation of the manuscript. A. Gadea and E. Farnea acknowledge the support of MICINN, Spain, and INFN, Italy, through the ACI2009-1070 bilateral action. A. Gadea activity has been partially supported by the Spanish MINECO under Grants No. AIC-D-2011-0746, No. AIC10-D-000568, and No. FPA2011-29854 and the Generalitat Valenciana under Grant No. PROMETEO/2010/101.

[1] A. M. Hoogenboom, E. Kashy, and W. W. Buechner, Phys. Rev. **128**, 305 (1962).
[2] P. Decowski, Nucl. Phys. A **169**, 513 (1971).
[3] A. S. Yousef, E. L. Sprenkel-Segel, and R. E. Segel, Phys. Rev. C **8**, 684 (1973).
[4] S. Piskor, P. Franc, W. Schäferlingová, and J. Kremének, Nucl. Phys. A **481**, 269 (1988).
[5] J. Kroon, B. Hird, and G. C. Ball, Nucl. Phys. A **204**, 609 (1973).
[6] J. A. Rice, B. H. Wildenthal, and B. M. Preedom, Nucl. Phys. A **239**, 189 (1975).
[7] L. Broman, C. M. Fou, and B. Rosner, Nucl. Phys. A **112**, 195 (1968).
[8] J. Vernotte *et al*., Phys. Rev. C **13**, 461 (1976).
[9] G. J. Costa *et al*., Nucl. Phys. A **256**, 277 (1976).
[10] J. Hermans *et al*., Nucl. Phys. A **284**, 307 (1977).
[11] P. J. Nolan *et al*., J. Phys. (London) A**6**, L37 (1973).
[12] P. M. Endt, Nucl. Phys. A **521**, 1 (1990), and references therein.
[13] P. M. Endt, Nucl. Phys. A **633**, 1 (1998), and references therein.
[14] N. Nica, J. Cameron, and B. Singh, Nucl. Data Sheets **113**, 1 (2012), and references therein.
[15] P. Mason *et al*., Phys. Rev. C **71**, 014316 (2005).
[16] M. Ionescu-Bujor *et al*., Phys. Rev. C **73**, 024310 (2006).
[17] F. Della Vedova *et al*., Phys. Rev. C **75**, 034317 (2007).
[18] C. Rossi Alvarez, Nucl. Phys. News **3**, 10 (1993).
[19] T. Yamazaki, Nucl. Data A **3**, 1 (1967).
[20] M. Piiparinen *et al*., Nucl. Phys. A **605**, 191 (1996).
[21] M. Weiszflog *et al*., Eur. Phys. J. A **11**, 25 (2001).
[22] W. D. Hamilton, *The Electromagnetic Interaction in Nuclear Spectroscopy* (North-Holland, Amsterdam; American Elsevier, New York, 1975), Chap. 12.
[23] P. M. Endt, At. Data Nucl. Data Tables **23**, 3 (1979).
[24] E. K. Warburton, J. W. Olness, A. R. Poletti, and J. J. Kolata, Phys. Rev. C **14**, 996 (1976).
[25] C. J. Van Der Poel *et al*., Nucl. Phys. A **373**, 81 (1982).
[26] J. C. Wells and N. R. Johnson, Report No. ORNL-6689, 1991, p. 44.
[27] J. F. Ziegler, *The Stopping and Range of Ions in Matter*, Vols. 3 and 5 (Pergamon Press, Oxford, 1980).
[28] J. F. Ziegler, J. P. Biersack, and V. Littmark, *The Stopping Power and Range of Ions in Solid* (Pergamon Press, Oxford, 1985).
[29] L. C. Northcliffe and R. F. Schilling, Nucl. Data, Sect. A **7**, 233 (1970).
[30] S. H. Sie, D. Ward, J. S. Geiger, R. L. Graham, and H. R. Andrews, Nucl. Phys. A **291**, 443 (1977).
[31] E. Caurier and F. Nowacki, Acta Phys. Pol. B **30**, 705 (1999).
[32] B. H. Wildenthal, Prog. Part. Nucl. Phys. **11**, 5 (1984).
[33] M. Bouhelal, F. Haas, E. Caurier, F. Nowacki, and A. Bouldjedri, Nucl. Phys. A **864**, 113 (2011).
[34] E. Caurier, K. Langanke, G. Martínez-Pinedo, F. Nowacki, and P. Vogel, Phys. Lett. B **522**, 240 (2001).
[35] M. Ionescu-Bujor *et al*., Phys. Rev. C **80**, 034314 (2009).